XPS Study of Ion Irradiated and Unirradiated UO$_2$ Thin Films

Yuri A. Teterin,[†,‡] Aleksej J. Popel,[§,]* Konstantin I. Maslakov,[†] Anton Yu. Teterin,[‡] Kirill E. Ivanov,[‡] Stepan N. Kalmykov,[†, ‡] Ross Springell,[#] Thomas B. Scott,[#] Ian Farnan[§]

[†]*Chemistry Department, Lomonosov Moscow State University, Moscow,* 119991, *Russia*
[‡]*NRC "Kurchatov Institute", Moscow, 123182, Russia*
[§]*Department of Earth Sciences, University of Cambridge, Downing Street, Cambridge, CB2 3EQ, UK*
[#]*Interface Analysis Centre, School of Physics, University of Bristol, Bristol, BS8 1TL, UK*

1

ABSTRACT: XPS determination of the oxygen coefficient $k_O=2+x$ and ionic (U^{4+}, U^{5+} and U^{6+}) composition of oxides UO_{2+x} formed on the surfaces of differently oriented (hkl) planes of thin UO_2 films on LSAT ($Al_{10}La_3O_{51}Sr_{14}Ta_7$) and YSZ (yttria-stabilized zirconia) substrates was performed. The U 4f and O 1s core-electron peak intensities as well as the U 5f relative intensity before and after the $^{129}Xe^{23+}$ and $^{238}U^{31+}$ irradiations were employed. It was found that the presence of uranium dioxide film in air results in formation of oxide UO_{2+x} on the surface with mean oxygen coefficients k_O in the range 2.07-2.11 on LSAT and 2.17-2.23 on YSZ substrates. These oxygen coefficients depend on the substrate and weakly on the crystallographic orientation.

On the basis of the spectral parameters it was established that uranium dioxide films AP2,3 on the LSAT substrates have the smallest k_O values, and from the XRD and EBSD results it follows that these samples have a regular monocrystalline structure. The XRD and EBSD results indicate that samples AP5-7 on the YSZ substrates have monocrystalline structure, however, they have the highest k_O values. The observed difference in the k_O values, probably, caused by the different nature of the substrates: the YSZ substrates provide 6.4% compressive strain, whereas (001) LSAT substrates result only in 0.03% tensile strain in the UO_2 films.

$^{129}Xe^{23+}$ irradiation (92 MeV, 4.8×10^{15} ions/cm^2) of uranium dioxide films on the LSAT substrates was shown to destroy both long range ordering and uranium close environment, which results in increase of uranium oxidation state and regrouping of oxygen ions in uranium close environment. $^{238}U^{31+}$ (110 MeV, 5×10^{10}, 5×10^{11}, 5×10^{12} ions/cm^2) irradiations of uranium dioxide films on the YSZ substrates were shown to form the lattice damage only with partial destruction of the long range ordering.

INTRODUCTION

Uranium dioxide, UO_2, is the main form of nuclear fuel used in the present generation of nuclear reactors. The knowledge and understanding of its in-reactor behavior and its stability under subsequent storage and disposal conditions are of great technological importance.[1,2]

The heat generated at nuclear power plants comes primarily from the slowing down of fission products with energies in the range 70 to 100 MeV. As a result, heat and radiation damage are produced inside the fuel pellets.[3,4,5]

Fresh fuel has close to stoichiometric ($UO_{2.001}$) composition. However, under in-reactor irradiation the fuel might develop an increased degree of non-stoichiometry.[1] Solubility and dissolution of uranium oxide in aqueous environment strongly depends on uranium valence state, as U(VI) is more soluble than U(IV) by many orders of magnitude.[6] Hence, the degree of non-stoichiometry in spent nuclear fuel has an important effect on its solubility and corrosion rate[7] which governs the release rate of the majority of radionuclides.[8]

This work considers the explicit effect of radiation damage by fission fragments on non-stoichiometry in spent nuclear fuel and outlines a methodology developed for determining the degree of non-stoichiometry in UO_{2+x}. For this purpose, thin films of UO_2 on LSAT (lanthanum strontium aluminum tantalum oxide) and YSZ (yttria-stabilised zirconia) substrates were produced and irradiated with Xe and U ions, respectively. The irradiated and unirradiated films were analyzed by EDX (Energy Dispersive X-ray spectroscopy), XRD (X-Ray Diffraction), EBSD (Electron Backscatter Diffraction), SEM (Scanning Electron Microscopy) and XPS technique. The obtained results were compared.

Previous papers considered mechanisms of xenon transfer and its interaction with uranium in UO_{2+x} (ref 9) theoretically, as well as the influence of defects[10,11] and pressure[12,13] on the ionic composition of these oxides. Adsorption energies of water on differently oriented uranium dioxide planes were calculated.[14,15,16]

The work on the study of the electronic structure of uranium and its alloys[17-21] and oxides UO_{2+x} ($x \leq 0$ and $x \geq 0$) employed theoretical calculation results,[22-34] photoelectron spectroscopy (PES)[35-41] and X-ray photoelectron spectroscopy (XPS) widely.[38,42-55] These techniques were used to study films on various substrates.[38-40,56-58]

Determination of uranium oxidation state and sample's ionic composition employs the U 4f doublet split due to the spin-orbit interaction by ΔE_{sl} (U4f)=10.8 eV.[17,50,59] The binding energy (BE) E_b(U $4f_{7/2}$) of the U $4f_{7/2}$ electrons in uranium and oxides grows as: ~377 eV (metallic U); ~380 eV (U^{4+}); ~381 eV (U^{5+}); ~382 eV (U^{6+}).[17,50,55,56,59,60,61,62] A special attention was paid to the study of mechanisms of structure formation, which leads to widening of main peaks and appearance of extra structure in the spectra.[50,59,63] The XPS spectra of some oxides exhibit typical shake-up satellites of about ~25% intensity of the basic peaks[41,51,60,64] The calculated spectroscopic factors f_{Anf} reflecting the fractions of the basic peak XPS intensities with the deduction of shake-up satellite intensities for the U 4f and U 5f peaks are: f_{U4f}=0.83 and f_{U5f}=0.86.[65,66] Shake-up satellites are located from the basic peaks toward the higher BE by ΔE_{sat}(U4f): ~7 eV (U^{4+}); ~8 eV (U^{5+}); ~4 eV and ~10 eV (U^{6+}).[60]

Since the U 4f BE on the moving from UO_2 to UO_3 changes by ΔE_b~2 eV, one can reliably determine uranium oxidation states for individual uranium oxides on the basis of the U $4f_{7/2}$ BE and positions (ΔE_{sat}) and relative intensities I_{sat} (%) of the shake-up satellites.[56,60]

The U 4f XPS structure is best resolved for the crystalline oxides. For complex amorphous oxides UO_{2+x} it is often difficult to segregate unambiguously the U 4f XPS peaks containing shake-up satellites into separate components for reliable quantitative information on uranium oxidation state and ionic composition of the studied oxide. Despite this, the XPS studies of uranium oxides by authors of refs 38,47,50,60,62 employed the U 4f XPS peak decomposition with shake-up satellite parameters in mind.

It is known that the traditional method of determination of the oxygen coefficient $k_O=2+x$ for UO_{2+x} based on the U 4f/O 1s XPS intensity ratio (with photoionization cross-sections or experimental sensitivity factors in mind) does not give satisfactory results (see ref 49). It is due to the fact that the O 1s intensity grows due to the presence of complex oxides UO_{2+x} as well as impurity oxides containing excess oxygen on the sample surface.

The valence electron BE range (0 - ~35 eV) in XPS of oxides UO_{2+x} changes significantly as the oxygen coefficient grows.[45] Thus, on the moving from UO_2 to γ-UO_3 in the outer valence molecular orbitals (OVMO) with BE range (0 - ~15 eV) a sharp U 5f peak disappears, and in the inner valence molecular orbitals (IVMO) with BE range (~15 - ~35 eV) instead of a single atomic U $6p_{3/2}$ peak two components appear.[42,61] Such a splitting is due to the IVMO formation in γ-UO_3.

The IVMO formation in uranium oxides due to interaction of the U 6p and O 2s atomic orbitals (AO) also results in formation of structure in other X-ray (emission, conversion, Auger) spectra of uranium oxides.[59,67,68,69] This structure parameters correlate with the uranium–oxygen interatomic distances in axial and equatorial directions in uranyl compounds and serve for quantitative determination of these compounds.[50,59]

The peak of the U 5f electrons weakly participating in chemical bond in UO_{2+x} is observed in the photoelectron[70] and X-ray photoelectron[52,53,54,68,69] spectra around zero BE. Spectra of compounds containing U(VI) do not exhibit this peak.[61] Therefore, the present work for determination of the oxygen coefficient $k_O=2+x$, uranium oxidation state and ionic composition $k(\%)$ of the studied oxides UO_{2+x} on the surface of single-crystalline films used the technique developed on the basis of the dependence of the U 5f peak relative intensity I_{5f} (rel. units) on the oxygen coefficient k_O.[44,45,49]

EXPERIMENTAL

Samples: Thin Films Production. Thin films of epitaxial UO_2 were produced by reactive sputtering onto LSAT and YSZ substrates with three different crystallographic orientations: (001), (110) and (111).[71]

A dedicated DC magnetron sputtering facility with UHV base pressure (10^{-9} mbar) was employed to grow the films. A depleted uranium metal target was used as a source of uranium. It was kept at a power of 50 W by controlled direct current of 0.11-0.14 A and the corresponding voltage of 350- 450 V, giving a growth rate of 0.9-1.1 Å/s for films on the LSAT substrates, and by controlled direct current at an average value of 0.15 A and the corresponding voltage of 330 V, giving a growth rate of about 1.5 Å/s for films on the YSZ substrates. Argon was used as the sputtering gas at a pAr in the range of 7 to 8×10^{-3} mbar. Oxygen was used as the reactive gas at a pO$_2$ in the range 3.4 to 4.4×10^{-5} mbar for films on the LSAT substrates and at a pO$_2$ of 2×10^{-5} mbar for films on the YSZ substrates, except for sample OB6 for which a pO$_2$ was 3×10^{-6} mbar. The LSAT and YSZ substrates were kept at a temperature close to 750 °C and to 600 °C, respectively.

The substrates were one side polished single crystal LSAT or YSZ with dimensions of 10×10×0.5 mm supplied by MTI Corp, USA. LSAT has a cubic perovskite structure with a_{LSAT}=3.868 Å,[72] and UO_2 has a cubic fluorite structure with a_{uo_2}=5.469 Å, both at room temperature.[71] This results in the epitaxial relationship in which the (001) plane of UO_2 is rotated by 45° in relation to the (001) plane of LSAT so that the (110) plane of UO_2, with a d-spacing $a_{uo_2}/\sqrt{2}$=3.867 Å, fits the LSAT (001) plane, with a d-spacing of 3.868 Å (=a_{LSAT}), as was described by Bao et al.[71] for a UO_2 film on a LaAlO$_3$ substrate. This causes the UO_2 lattice to be only at a slight tension of +0.03% with respect to the substrate in-plane spacing. This 45° rotation epitaxial relationship only holds between the LSAT and UO_2 (001) planes. YSZ has a cubic fluorite structure with a_{YSZ}=5.139 Å.[73] This results in the plane to plane epitaxial match in which the plane of UO_2 is put at compression of -6.4% by the plane of YSZ. This plane to plane

epitaxial relationship holds for the (001), (110) and (111) plane orientations. Table 1 summarizes the produced samples. Sample pairs AP1/OB1 to AP4/OB4 were produced by cutting one sample into two halves using a diamond saw for various studies.

It was identified by means of EDX and XPS analyses that the films of uranium dioxide contain Nb. Based on the results from EDX, XRD, EBSD, SEM and XPS measurements, it is suggested that Nb is present in the form of Nb_2O_5 and is located in particulates, which precipitated onto the substrates during growth of the films. The particulates can be seen in SEM images (not shown) obtained at different angles. They have sizes down to 30 nm and are densely populated. Niobium concentration was determined by EDX technique, with the point-analysis spot size of 1-2 µm in diameter, at different locations on the surface of the films (~3.5 wt%) which agrees with the concentration values obtained from XPS (~5 wt%). Since the analysis spot in XPS is an ellipse with the minor and major axes of 300 µm and 700 µm, respectively, it was not possible to find an area free of niobium oxide. That is why Nb_2O_5 lines were observed in XPS spectra from the studied samples which had a relatively small width $\Gamma(Nb\ 3d_{5/2})$=1.2 eV and $E_b(Nb\ 3d_{5/2})$=206.9 eV. This agrees with the fact that the oxidation state of Nb in the samples is only Nb^{5+}. The work by Fu et al.[19] also shows that regions of UO_2 and Nb_2O_5 are formed during the oxidation of uranium-niobium alloy with oxygen. Niobium oxide is not observed in XRD scans of the samples, possibly, due to its low concentration in the films. This observation is consistent with the results obtained in the work by Strehle et al.,[73] where the co-deposition of U and Nd was performed onto YSZ substrates. The XRD scans did not exhibit any difference between pure UO_2 and $U_xNd_yO_z$ samples, which can be related to the absence of the crystal structure involving neodymium.

Crystallographic orientations for the UO_2 films were determined by means of XRD (θ-2θ scans with φ rotation) and EBSD techniques (not shown). In addition, UO_2 films on the (001) YSZ substrates, produced under similar conditions, were thoroughly characterized by Strehle et al.[73] and it was shown that these films are single crystals. Since the epitaxial relationship and lattice mismatch for the UO_2 films on the (111) and (110) YSZ substrates are the same as for the UO_2 films on the (001) YSZ substrate and based on the obtained XRD and EBSD results, it is possible to suggest that these films are also single crystals. Based on the expected epitaxial relationship for UO_2 films on the (001) LSAT substrates and the obtained XRD and EBSD results, we are inclined to suggest that the films on the (001) LSAT substrates can be considered as single crystals. As an example, Figure 1 illustrates a result of the EBSD study for sample AP2, which confirms formation mainly of a single crystal with the surface orientation (001). Sample AP3 provides similar results. Uranium dioxide films on the (111) and (110) LSAT substrates are described as preferentially oriented.
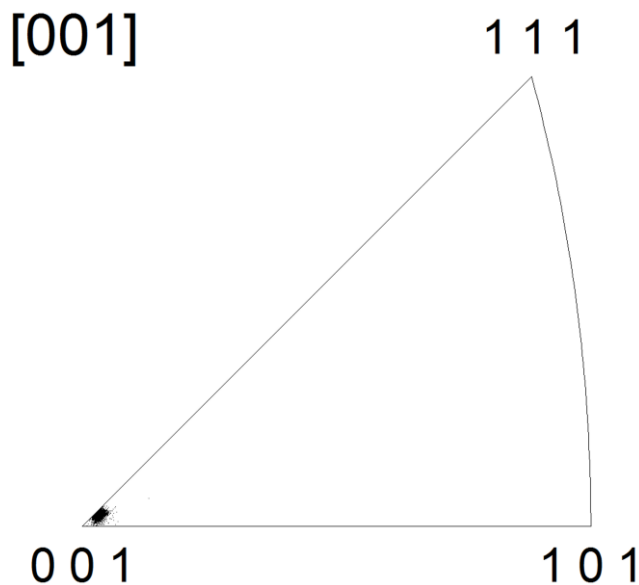
Figure 1. A triangular inverse pole figure for sample AP3 obtained from the EBSD study.

Film thickness for samples AP1 to AP4 was measured using transverse SEM on a cross section of the sample. Focused ion beam (FIB)-SEM was used to measure film thickness for samples OB6 and OB7 after they have been irradiated. Secondary ion mass spectrometry (SIMS) was performed on sample OB6 (after it has been irradiated) to verify the thickness measured with the FIB-SEM method and on sample AP6 to deduce its thickness, as it was not possible to resolve the UO_2 film in the FIB-SEM study, possibly, due to a low electrical conductivity of the film. Film thickness for samples AP5, OB5 and AP7 was estimated based on the growth rate calculated from the measured film thicknesses for samples AP6, OB6 and OB7 and the corresponding deposition times.

Table 1. Summary of the Produced Thin Film UO_2 Samples.

| Sample	LSAT (AP1-AP4) and YSZ (AP5-AP7, OB5-OB7) substrate crystallographic orientation (*hkl*)	UO_2 film orientation (*hkl*)	UO_2 film thickness (nm)
AP1	(111)	(210)[a]	110
AP2	(001)	(001)	140
AP3	(001)	(001)	120
AP4	(110)	(111)[a]	140
AP5	(001)	(001)	90
OB5	(001)	(001)	150
AP6	(110)	(110)	150
OB6	(110)	(110)	150
AP7	(111)	(111)	150
OB7	(111)	(111)	150

[a]Preferred crystallographic orientation of the as-produced samples

Sample Irradiations. Sample irradiations were performed on the IRRSUD beamline at the GANIL accelerator, Caen, France. UO_2 films on the LSAT substrates (OB1-4) were irradiated with $^{129}Xe^{23+}$ ions of 92 MeV energy to a fluence of 4.8×10^{15} ions/cm^2 to simulate the damage produced by fission fragments in nuclear fuel. The energy and mass of the ions used for the irradiation is representative of the typical fission fragments.[4,5] The flux was kept at around 1.3×10^{10} ions/(cm^2 s) which caused heating of the samples to a temperature not exceeding 150

°C. The samples were allowed to cool down to ambient temperature (around 19 °C) before the beamline was brought to atmospheric pressure using nitrogen gas to minimize surface oxidation of the samples. UO_2 films on the YSZ substrates were irradiated with $^{238}U^{31+}$ ions of 110 MeV energy to fluences of 5×10^{10} (OB5), 5×10^{11} (OB6) and 5×10^{12} (OB7) ions/cm^2 to induce radiation damage. The flux was kept at around 1×10^8 ions/(cm^2 s). The irradiation was conducted at an ambient temperature of 16-17 °C. No heating of the samples was observed. The beam line base vacuum was 6×10^{-7} mbar during the irradiations.

According to the SRIM-2012.03 software,[74] the nuclear and electronic stopping, dE/x, for 92 MeV $^{129}Xe^{23+}$ ions in UO_2 is 0.26 and 24.6 keV/nm, respectively, and the projected range is 6.5 μm and for 110 MeV $^{238}U^{31+}$ ions is 0.96 and 27.4 keV/nm, respectively, and the projected range is 6.7 μm. A theoretical UO_2 density of 10.96 g/cm^3 (ref 5) was assumed in the SRIM calculation. The SRIM results indicate that the $^{129}Xe^{23+}$ and $^{238}U^{31+}$ ions completely penetrate the UO_2 thin films (150 nm max) and the electronic stopping regime dominates the dissipation of ion energy throughout the entire film.

X-ray Photoelectron Measurements. XPS spectra of UO_{2+x} were recorded on a Kratos Axis Ultra DLD spectrometer using monochromatic Al-Kα radiation (hv=1486.6 eV) at 150 W X-ray gun power under 1.3×10^{-7} Pa at room temperature (Figure 2). The analyzed area was an ellipse with 300 and 700 μm minor and major axes, respectively. Binding energy scale of the spectrometer was preliminarily calibrated by the position of the peaks of Au $4f_{7/2}$ (83.96 eV) and Cu $2p_{3/2}$ (932.62 eV) core levels for pure gold and copper metals. The spectra were acquired in the constant analyzer energy mode using a pass energy of 20 eV and a step size of 0.05 eV. The equipment resolution measured as the full width on the half-maximum (FWHM) of the Au $4f_{7/2}$ peak was less than 0.65 eV. The binding energies (BE) were measured relatively to the BE of the C 1s electrons from hydrocarbons adsorbed on the sample surface that was accepted to be equal to 285.0 eV. The FWHMs are given relatively to that of the C 1s XPS peak from hydrocarbon on the sample surface being 1.3 eV.[50] The error in the determination of the BE and the peak width did not exceed ±0.05 eV, and the error of the relative peak intensity − ±5%. The inelastically scattered electrons-related background was subtracted with the Shirley method.[75]
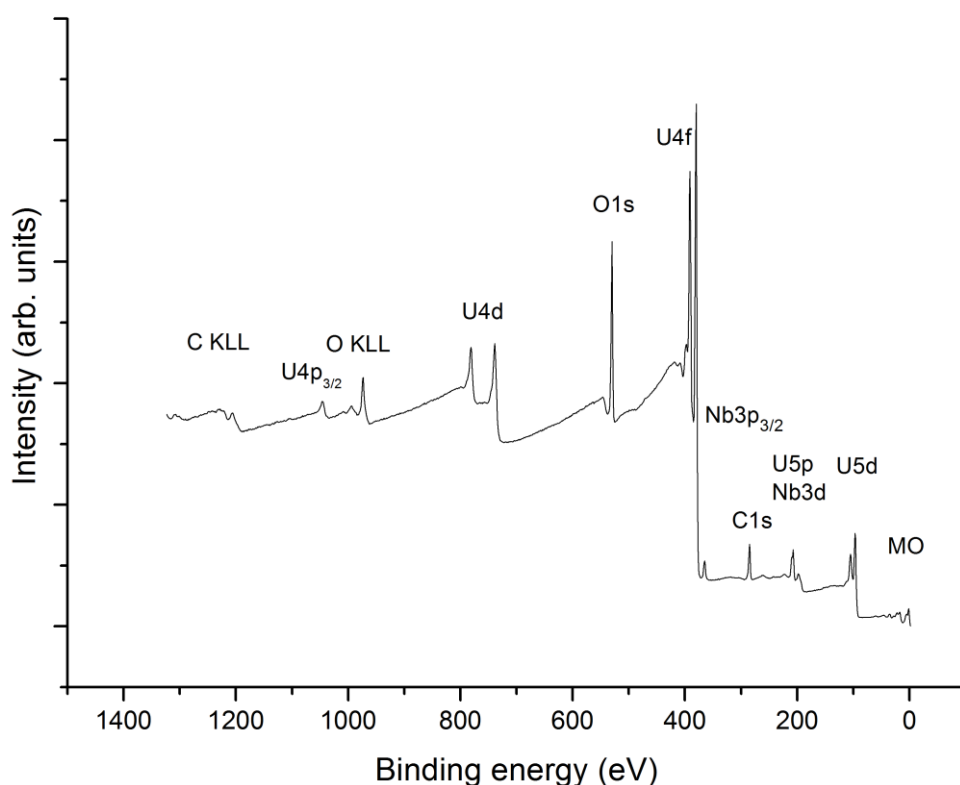
Figure 2. A survey XPS scan from a UO_2 film (sample AP3).

$^{40}Ar^+$ etching of 2×2 mm^2 sample area was conducted at the accelerating voltage of 2 kV and beam current of 50 μA at 3×10^{-7} Pa and room temperature. The etching rate was 7.1 nm/min for SiO$_2$ under these conditions. Thus, UO$_2$ film on the YSZ substrate (AP7) was Ar$^+$ etched at 2 keV and 3×10^{-7} Pa. The flux was maintained at about 3.1×10^{14} ions/(cm^2 s).

The quantitative elemental analysis was performed for several nanometer-deep layers of the studied samples. It was based on the fact that the spectral intensity is proportional to the number of certain atoms in the studied sample. The following ratio was used: $n_i/n_j=(S_i/S_j)(k_j/k_i)$, where n_i/n_j is the relative concentration of the studied atoms, S_i/S_j is the relative core-shell spectral intensity, k_j/k_i is the relative experimental sensitivity coefficient. The following coefficients relative to the C 1s were used: 1.00 (C 1s); 2.81 (O 1s); 10.51 (Nb3d); 36.0 (U 4f$_{7/2}$; see ref 76).

Determination of the Oxygen Coefficient $k_O=2+x$ and Ionic Composition of Oxides UO$_{2+x}$. Once uranium oxide UO$_{2+x}$ contains uranium ions of different oxidation states, the U 4f XPS spectrum is expected to consist of several peaks at different BEs. Usually, these peaks are superimposed because of low equipment resolution. This widens and distorts the shape of the main peak, which complicates its decomposition into components. The O 1s intensity in this case is usually higher due to oxygen-containing impurities on the surface. This increases the error in the oxygen coefficient $k_O=2+x$ determination, which is found from the U 4f/O 1s intensity ratio with sensitivity coefficients in mind. In this case we can only yield a qualitative interpretation of the results (Table 2, column 3).

Determination of uranium ions composition on the basis of intensities of U 4f-electron lines was carried out based on the known parameters of the spectra of uranium oxides. Both the primary and satellite peaks for U 4f were used in the fitting procedure. The binding energy of the U 4f$_{7/2}$ electrons was taken as: ~380 eV (U^{4+}); ~381 eV (U^{5+}); ~382 eV (U^{6+}) and shake-up satellites located from the basic peaks toward the higher BE by: ~7 eV (U^{4+}); ~8 eV (U^{5+}); ~4 eV and ~10 eV (U^{6+}) were used, as was described in Section I. Although, it is known that the FWHM, Γ(U 4f7/2), of U 4f$_{7/2}$-line decreases as: ~1.5 eV (U^{4+}); ~1.4 eV (U^{5+}) and ~1.2 eV (U^{6+}), related to multiplet splitting and decrease of unpaired U 5f-electrons from 2 to 0, the FWHM value of 1.4 eV was taken for fitting the U^{4+}, U^{5+} and U^{6+} curves to simplify the fitting. The curve shapes were approximated by a mixed Gaussian (~80%) and Lorentzian (~20%) function to get the best fit to the experimental curve. In the cases when some peaks were absent, the initial % composition was determined based on the method of U 5f/U 4f$_{7/2}$-electron intensities (our suggested method), followed by an iterative fitting procedure to obtain a final fit. The results obtained by the spectra fitting procedure are shown in the parentheses in Table 2 in the fourth column.

Table 2. Surface Elemental Composition of the Epitaxial UO_{2+x}[a] Thin Films, Peak Intensity of the U 5f Electrons[b], Oxygen Coefficient k_O[c] in UO_{2+x} Oxide, Composition of Uranium Ions $k(\%)$[d] of Unirradiated (AP1-7) and $^{129}Xe^{23+}$ (OB1-4), and $^{238}U^{31+}$ (OB5-7) Irradiated Thin Films of Uranium Dioxide.

No.	Sample (*hkl*)	Elemental composition UO_{2+x}	I_{U5f} (±0.001)	k_O in UO_{2+x} (± 0.01)	k U^{4+}	U^{5+}	U^{6+}
1	AP1 (210)[e] OB1	$UO_{2.8}$ UO_{47}	0.025 0.013	2.11 2.31	44 (45) 0.3	45 (40) 68	11 (15) 31
2	AP2 (001) OB2	$UO_{3.5}$ UO_{21}	0.029 0.025	2.07 2.11	58 (60) 44	35 (36) 45	7 (4) 11
3	AP3 (001) OB3	$UO_{3.6}$ UO_{15}	0.028 0.023	2.08 2.14	52 (58) 33	39 (38) 52	9 (4) 14
4	AP4 (111)[e] OB4	$UO_{3.9}$ UO_{15}	0.027 0.021	2.10 2.17	48 (54) 25	42 (41) 57	10 (5) 17
5	AP5 (001) OB5 (001)	$UO_{3.4}$ $UO_{3.4}$	0.021 0.022	2.17 2.15	25 (47) 32 (45)	57 (48) 53 (47)	17 (5) 15 (8)
6	AP6 (110) OB6 (110)	$UO_{3.2}$ $UO_{3.2}$	0.017 0.021	2.23 2.17	13 (37) 25 (44)	64 (55) 57 (48)	23 (8) 17 (8)
7	AP7 (111) OB7 (111) AP7(Ar+)[f]	$UO_{3.6}$ $UO_{3.4}$ $UO_{1.98}$	0.019 0.020 0.025	2.20 2.18 2.11	18 (44) 23 (48) 42	61 (48) 59 (45) 47	21 (8) 18 (7) 11

[a]Elemental composition obtained on the basis of the core line U 4f$_{7/2}$, and O 1s intensities of uranium dioxide and atomic photoionization cross-sections σ: 0.70 (O 1s); 9.0 (U 4f$_{7/2}$).
[b]Peak intensity of the U 5f electrons measured as a ratio: $I_{U5f}= I(U\ 5f)/I(U\ 4f_{7/2})$ without taking into account intensities of the shake-up satellites.
[c]Oxygen coefficient $k_O = 2+x$ in UO_{2+x} oxide found from Equation 1.
[d]Composition of uranium ions k (%) found by using Equations (4) – (6); the values obtained based on dividing the U 4f$_{7/2}$ peak into components and intensities of the shake-up satellites are shown in the parentheses.
[e]Preferred crystallographic orientation.
[f]Sample AP7 after the 180 sec Ar$^+$ treatment.

The oxygen coefficient $k_O=2+x$ and ionic composition of UO_{2+x} can be also determined on the basis of the intensity of the peak of the U 5f electrons not participating in the chemical bonding. The present work physically grounded this technique and considered it in more details than before.[44,45,49] This technique considers oxygen ions bound with uranium ions immediately. Adsorbed oxygen ions not participating in uranium-oxygen bonding do not affect the U 5f intensity; however, they affect strongly the uranium/oxygen ratio on the surface, which practically does not allow the traditional XPS quantitative analysis to be used. The U 5f electrons

weakly participating in chemical bonding in uranium oxides are strongly localized and observed as a sharp peak at the lower BE side from the outer valence band (see Figure 3). The XPS from γ-UO$_3$ not containing the U 5f electrons does not exhibit this peak.[61] Since the U 5f BE is about ~3 eV lower than that of the low energy OVMO band edge ("quasi-gap"), one can suggest that the U 5f intensity must decrease discretely as uranium oxidation state grows from U^{4+} to U^{5+} and U^{6+}, since the U 5f electrons transit from the localized state to the outer valence band. The U 5f intensity must first decrease twice and then vanish (Figure 3). Indeed, this was observed in the XPS of neptunium compounds, as neptunium oxidation state increased from Np(5f^2)$^{5+}$ to Np(5f^1)$^{6+}$ (ref 50). Therefore, the U 5f intensity can be used as a quantitative parameter of the number of U 5f electrons involved in chemical bonding in uranium oxides.
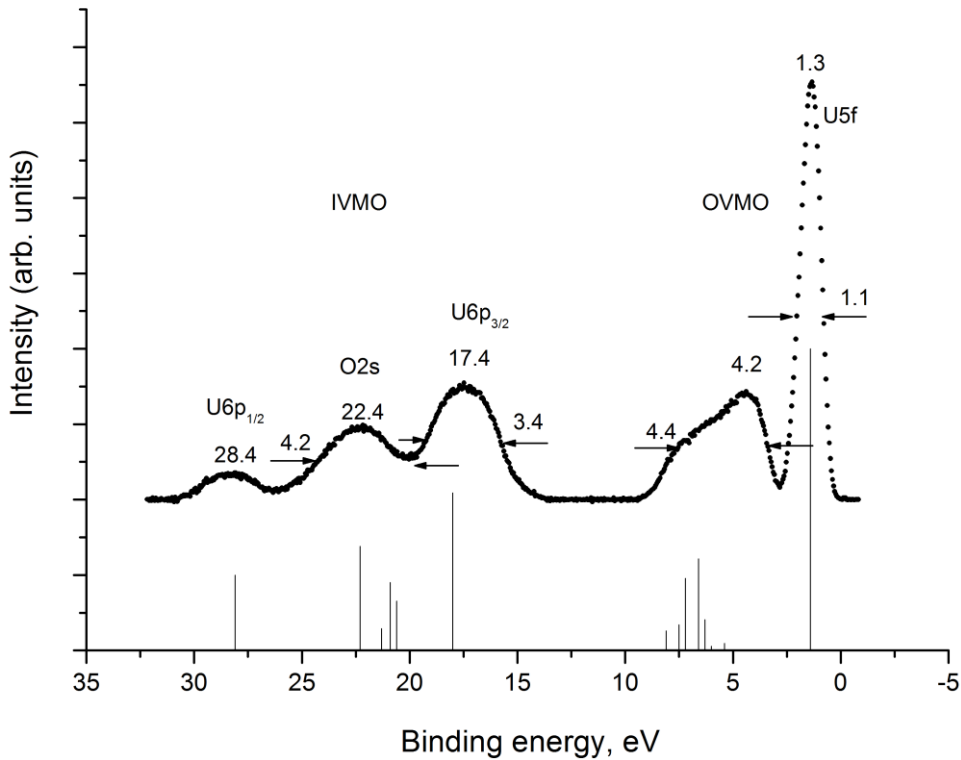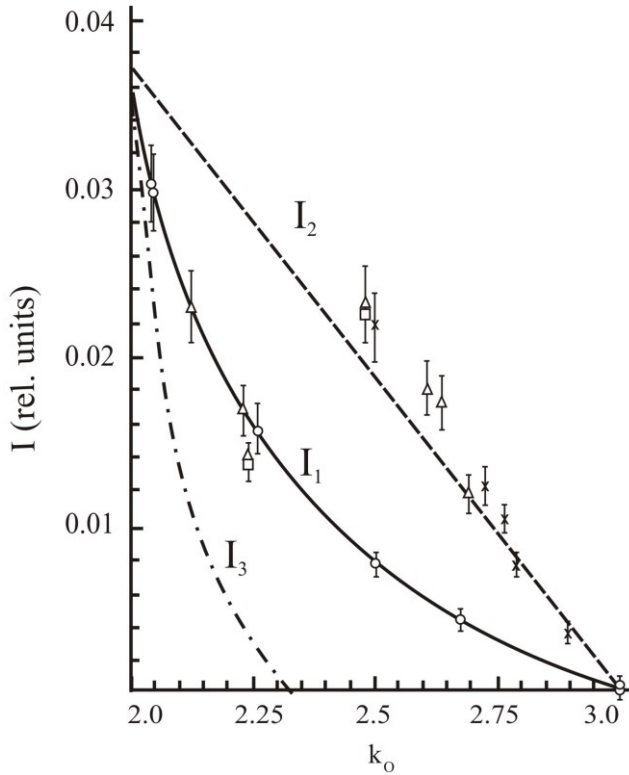

Figure 3. A valence XPS scan from a UO$_2$ film (sample AP3). Vertical bars show the calculated spectrum for the UO$_8$$^{12-}$ (O$_h$) cluster reflecting uranium close environment in UO$_2$ (ref 42).

The relative U 5f intensity I_l (rel. units) determined as the U 5f/U 4f$_{7/2}$ intensity ratio without the shake-up satellites can be presented as dependence on the oxygen coefficient k_O=2+x (Figure 4). For synthetic and natural oxides it is:[44,45]

$$I_l = 5.366 \, k_O^{-7.173} \tag{1},$$

which is in a good agreement with the dependence of the magnetic susceptibility on the oxygen coefficient.[50,77]. This agreement is not unexpected since the U 5f intensity is proportional to the number of the U 5f electrons responsible for the magnetic properties.

Figure 4. Dependence of the relative U 5f XPS intensity (I) on the oxygen coefficient (k_O=2+x) for UO$_{2+x}$: I_1 (Eq.(1)); I_2 (Eq.(2)); I_3 (Eq.(3)); o – synthetic oxides; Δ, $\square$- uraninites; x – mixtures of UO$_2$ and γ-UO$_3$ (ref 45).

The value $I_1(2)$=0.0383 for UO$_2$ was found by the extrapolation of dependence (I_1) at $k_O{\rightarrow}2$ (Figure 4). It differs from the value 0.0372 found from (1). The value $I_1(3)$=0.002 is not zero at $k_O{\rightarrow}3$ because it is difficult to describe the experimental curve (Figure 4) with the analytical function (1). Therefore, at $k_O{\rightarrow}2$ and 3 the use of dependence (1) must lead to increase of the error.

With $I_1(2)$ = 0.0383 in mind, a dependence of I_2 reflecting the expected change of the U 5f intensity on the oxygen coefficient k_O for the mixtures of UO$_2$ and UO$_3$ was built as:

$$I_2 = - 0.0383\, k_O + 0.1149 \qquad (2).$$

This dependence is in a satisfactory agreement with the corresponding experimental data on UO$_2$ and UO$_3$ mixtures (Figure 4). Decrease of I_2 as k_O grows is due to the increase of concentration of the U^{6+} ions that do not contribute to the U 5f intensity.

The difference ΔI=I_2–I_1 characterizes the decrease of the U^{4+} concentration in complex oxides UO$_{2+x}$ as k_O grows. Having suggested that synthetic oxides contain only uranium ions of formal oxidation states U^{4+}, U^{5+}and U^{6+} with electronic configurations U5f^2, U5f^1 and U5f^0 respectively, one can find a dependence of decrease of intensity I_3 due to the U^{4+} ions as k_O grows:

$$I_3 = I_2 - 2(I_2 - I_1) = 2I_1 - I_2 \qquad (3).$$

This dependence shows (see Figure 4) that as the k_O grows from 2 to 2.35 the U^{4+} ions in UO$_{2+x}$ vanish. This agrees with the XRD data showing that in synthetic oxides at $k_O{\rightarrow}2.38$ the UO$_2$ structure containing the U^{4+} ions vanishes.[78]

In this approximation, expressions (1-3) and Figure 4 enable to determine the oxygen coefficient k_O and ionic composition in UO$_{2+x}$.

Indeed, if the value I_1 is known from the experiment, the values I_2 and I_3 can be found from (2) and (3), and fractions ν (U^{n+}) of uranium ions of different oxidation states can be found from:

$$\nu_1\ (U^{4+}) = I_3/0.0383 \qquad\qquad (4),$$
$$\nu_2\ (U^{5+}) = 2(I_2 - I_1)/0.0383 \qquad\qquad (5),$$

11

$$\nu_3 (U^{6+}) = (0.0383 - I_2)/0.0383 \qquad (6).$$

In this case we can obtain repetitive data agreeing with other studies results.[50] The data obtained using expressions (1-6) are given in Table 2. In such an approximation the U^{5+} state was considered as a spectroscopic state for dependence of I_1 where the oxygen coefficients were obtained using chemical methods.[45] The U^{5+} ions were suggested to appear in UO_2 (CaF_2) lattice due to increase of some of U-O interatomic distances without changes in the stoichiometric composition of UO_2. Physically it means that in the U(IV)O_2 phase another phase U(V)O_2 forms without changes in oxygen content. It leads to disappearance of CaF_2 lattice in UO_{2+x} as the oxygen coefficient grows, which agrees with the XRD data.[78] Therefore, in order to deduce the oxygen coefficient k_O from the ion fractions ν_i (4,5,6) one has to multiply by 2 (the number of oxygens in UO_2) the sum of fractions $[\nu_1(U^{4+}) + \nu_2(U^{5+})]$ and to add the fraction $\nu_3(U^{6+})$ multiplied by 3 (the number of oxygens in UO_3) (see Table 2). The error in the fractions of UO_{2+x} ionic composition has to be taken into account.

RESULTS AND DISCUSSION

Determination of uranium oxidation state and UO_{2+x} ionic composition, as mentioned above, employs both the traditional XPS parameters (BEs and peak intensities) and the structure parameters of the core- and valence spectra such as: U 5f relative intensity; OVMO (IVMO) – core level BE differences; spin-orbit splitting ΔE_{sl} (eV) and multiplet splitting ΔE_{ms} (eV); dynamic effect – related structure parameters; relative positions of core-level shake-up satellites ΔE_{sat} (eV).[50] These XPS parameters allow getting information on uranium physical and chemical properties in the studied samples.

The surface treatment with Ar^+ ions was not used during the XPS study of the films in this work, as it is known that Ar^+ etching can change ionic composition of the surface. Since the data from the surface etched by Ar^+ can be useful in discussing the results of the study of the radiation damage of the uranium dioxide films, thus, for sample AP7 the effect of Ar^+ etching on the surface composition was studied. It was found that after the 20 sec etching the C 1s intensity became ~10 times lower, and the O 1s peak became single with Γ(O1s)=1.2 eV. The U 4f spectrum was observed as a spin-orbit split (ΔE_{sl}=10.8 eV) of 1.8 eV wide doublet with symmetrical peaks. Intensity of the shake-up satellites ($I_{sat}=I_s/I_o$), equal to the ratio of the satellite area (I_{sat}) to the area of the basic peak (I_o), was observed to have 30% intensity at ΔE_{sat1}= 6.9 eV. This structure is typical for UO_2 (ref 50)]. After the 60-120-180 sec etching and staying for a while in the spectrometer chamber ("annealing") the XPS structure did not change significantly. After the 180 sec etching the U $4f_{7/2}$ XPS exhibited a weak shoulder at the lower BE side attributed to metallic U. For the 180 sec etching the oxygen coefficient k_O was 1.98 based on the U 4f and O 1s intensities. The same coefficient found on the basis of the U 5f intensity was 2.11. The ionic composition of the sample was found to be: 42%(U^{4+}), 47%(U^{5+}) and 11(U^{6+}) (Table 2). This unexpected result agrees with the fact that uranium oxides can self-organize and form a stable lattice UO_{2+x} containing different phases.[78,79] This must be taken into account in the studies of irradiation of UO_2 films with xenon and uranium ions.

The survey XPS spectrum (Figure 2) provides important information on the studied sample. It consists of peaks of included elements and is typical for uranium oxide. This spectrum also contains the Auger peaks of carbon (C KLL), oxygen (O KLL) and the XPS peak at 207.1 eV identified as the Nb $3d_{5/2}$ peak of niobium in Nb_2O_5 (ref 80). Niobium impurity formed during the sample preparation. The Nb $3p_{3/2}$ peak of Nb_2O_5 was observed at E_b(Nb$3p_{3/2}$)=362.7 eV. Despite the fact that the Nb $3p_{1/2}$ peak of Nb_2O_5 at E_b(Nb $3p_{1/2}$)=378.2 eV is superimposed with the U $4f_{7/2}$ peak at E_b(U $4f_{7/2}$)≈379.9 eV (Table 3), the Nb $3p_{1/2}$ intensity does not contribute significantly (within the error) to the U $4f_{7/2}$ intensity since the Nb $3p_{1/2}$ peak has many times lower intensity than the U $4f_{7/2}$ one because the U $4f_{7/2}$ photoionization cross-section is ~10 times higher than the Nb $3p_{1/2}$ one,[81] and uranium content is many times higher than niobium content.

The XPS spectra are shown in Figures 2,3,5,6 and 7, and the corresponding BE are given in Table 3.

Table 3. Electron Binding Energy $E_b{}^a$ (eV), Line Width Γ^b (eV) in the Parentheses, Satellite Positions $\Delta E_{sat}{}^c$ (eV) of Unirradiated (AP1-4 on LSAT and AP5-7 on YSZ) and $^{129}Xe^{23+}$ (OB1-4) and $^{238}U^{31+}$ (OB5-7) Irradiated Thin Films of Uranium Dioxide.

No	Sample (*hkl*)	U 5f	U 4f$_{7/2}$ U^{4+}	U 4f$_{7/2}$ U^{5+}	U 4f$_{7/2}$ U^{6+}	Γ U 4f$_{7/2}$	O 1s
1	AP1 (210)^d	1.2(1.2)	379.7(1.4) 6.8(3.0)	380.9(1.4) 7.9(2.1)	382.2(1.4)	2.1	529.8(1.1)
	OB1	1.3(1.2)		380.4(1.5)		1.6	530.1(1.4)
2	AP2 (001)	1.3(1.2)	379.7(1.4) 6.8(2.0)	380.9(1.4) 7.9(2.0)	382.2(1.4)	2.3	529.7(1.1)
	OB2	1.2(1.2)		380.4(1.9)		1.9	530.1(1.5)
3	AP3 (001)	1.3(1.1)	379.9(1.4) 6.8(1.9)	381.1(1.4) 7.9(2.1)	382.4(1.4)	2.2	530.1(1.0)
	OB3	1.0(1.2)		380.3(2.0)		2.0	529.8(1.4)
4	AP4 (111)^d	1.2(1.2)	379.7(1.4) 6.8(1.9)	380.8(1.4) 8.0(2.1)	382.1(1.4)	2.3	529.7(1.1)
	OB4	1.3(1.1)		380.5(1.8)		1.8	530.1(1.4)
5	AP5 (001)	1.6(1.0)	380.3(1.8) 6.1 (2.1)	381.4(1.8) 7.5(2.1)	383.3(1.8)	2.5	530.1(1.1)
	OB5 (001)	1.5(1.1)	380.1(1.5) 6.2(2.1)	381.2(1.5) 7.7(2.1)	382.7(1.5)	2.5	530.1(1.1)
6	AP6 (110)	1.6(1.1)	380.2(1.6) 6.0(2.5)	381.4(1.6) 7.6(2.3)	382.9(1.6)	2.4	530.2(1.2)
	OB6 (110)	1.5(1.0)	380.1(1.6) 6.1(2.1)	381.2(1.6) 7.7(2.1)	382.8(1.6)	2.3	530.1(1.1)
7	AP7 (111)	1.5(1.1)	380.0(1.5) 6.1(2.1)	381.2(1.5) 7.7(2.1)	382.7(1.5)	2.4	530.1(1.1)
	OB7 (111)	1.4(1.2)	380.0(1.5) 6.6(2.3)	381.1(1.5) 7.6(2.6)	382.6(1.5)	2.4	530.0(1.1)
	AP7(Ar+)^e	1.2(1.6)	379.8(1.6)	381.5(1.7)		1.6	530.0(1.2)

^{a}1-st peak – binding energy measured relative to the E_b (C1s)=285.0 eV of hydrocarbons on the sample surface.
^{b}Line width reported relative to the Γ(C 1s) =1.3 eV in the parentheses.
^{c}2-nd peak – satellite energy ΔE_{sat} relative to the basic peak.

Valence Electron Spectra Range. The valence bands of the studied samples were observed in the BE range 0 - ~35 eV. They consist of the OVMO (0 - ~15 eV BE) and IVMO (~15 - ~35 eV BE) ranges,[42] (Figure 3). Peaks in the U 6p – O 2s BE range are relatively wide and structured comparing to the corresponding core U 4f and O 1s ones (Table 3, Figures 5 and 6). This contradicts the Heisenberg uncertainty ratio $\Delta E \Delta \tau \approx h/2\pi$, where ΔE is the natural width of a level from which an electron was extracted, $\Delta \tau$ is the hole lifetime and h is the Planck constant. Since the hole lifetime ($\Delta \tau$) grows as the absolute atomic level energy decreases, the lower BE XPS atomic peaks are expected to be narrower. In particular, if the O 2s level was atomic, its FWHM would be lower than that of the O 1s peak being Γ(O 1s)=1.0 eV (Table 3, Figure 5), which contradicts the experimental data. Taking into account the data on UO_2 (refs 42 and 45), the O 2s and U 6p levels were shown not to be atomic, but the IVMO-related. The calculated results of the electronic structure of the cluster $UO_8{}^{12-}$, representing uranium close environment in UO_2, are presented under the spectrum of valence electrons (Figure 3). These results were obtained in approximation of the relativistic method of discrete variation (RDV).[42]
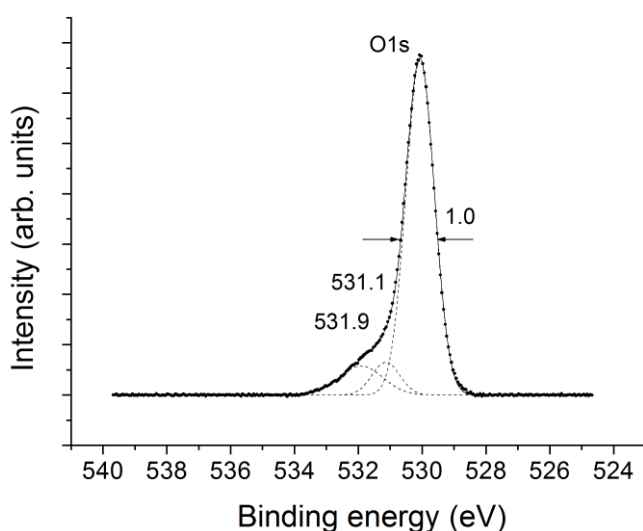
Figure 5. An XPS narrow-scan O 1s from a UO_2 film (sample AP3).

The valence bands of the studied samples AP1-7 and OB1-7 are formed mostly from the U 6s,6p,6d,5f,7s,7p and O 2s,2p electrons. The OVMO structure is mostly formed from the U 6d,5f,7s,7p – O 2p interaction, while the IVMO structure is mostly formed from the U 6s,6p – O 2s-interaction.[42,45] The IVMO-related structure of the studied samples is a superposition of the IVMO-related structures of different uranium oxides. Although complicated, this structure provides the qualitative and quantitative information on the UO_{2+x} physical and chemical properties[50] (Figure 3).

For example, intensity of the sharp (Γ(U 5f)=1.1 eV) single peak of the weakly bound quasiatomic U 5f electrons observed at ΔE_b(U 5f)=1.3 eV is an important parameter. The relative U 5f intensity ($I_{U\,5f}$) found as a ratio of the U 5f to the U $4f_{7/2}$ intensities according to Expression 1 allows oxygen coefficients (k_O,%) to be calculated for uranium oxides UO_{2+x} (Table 2). With Expressions 2-6 in mind, it allowed to find the relative content of uranium ions (k) of different oxidation states U^{4+}, U^{5+} and U^{6+}. These data are given in Table 2 for each sample. This table also contains crystallographic (*hkl*) indices of the uranium dioxide films and elemental composition of UO_{2+x} found based on the O 1s and U $4f_{7/2}$ peak intensities and the corresponding sensitivity coefficients. The ionic composition of the surface found based on the results of decomposition of the U 4f spectrum into the constituent elements (Figure 6,7) is presented in the parentheses.
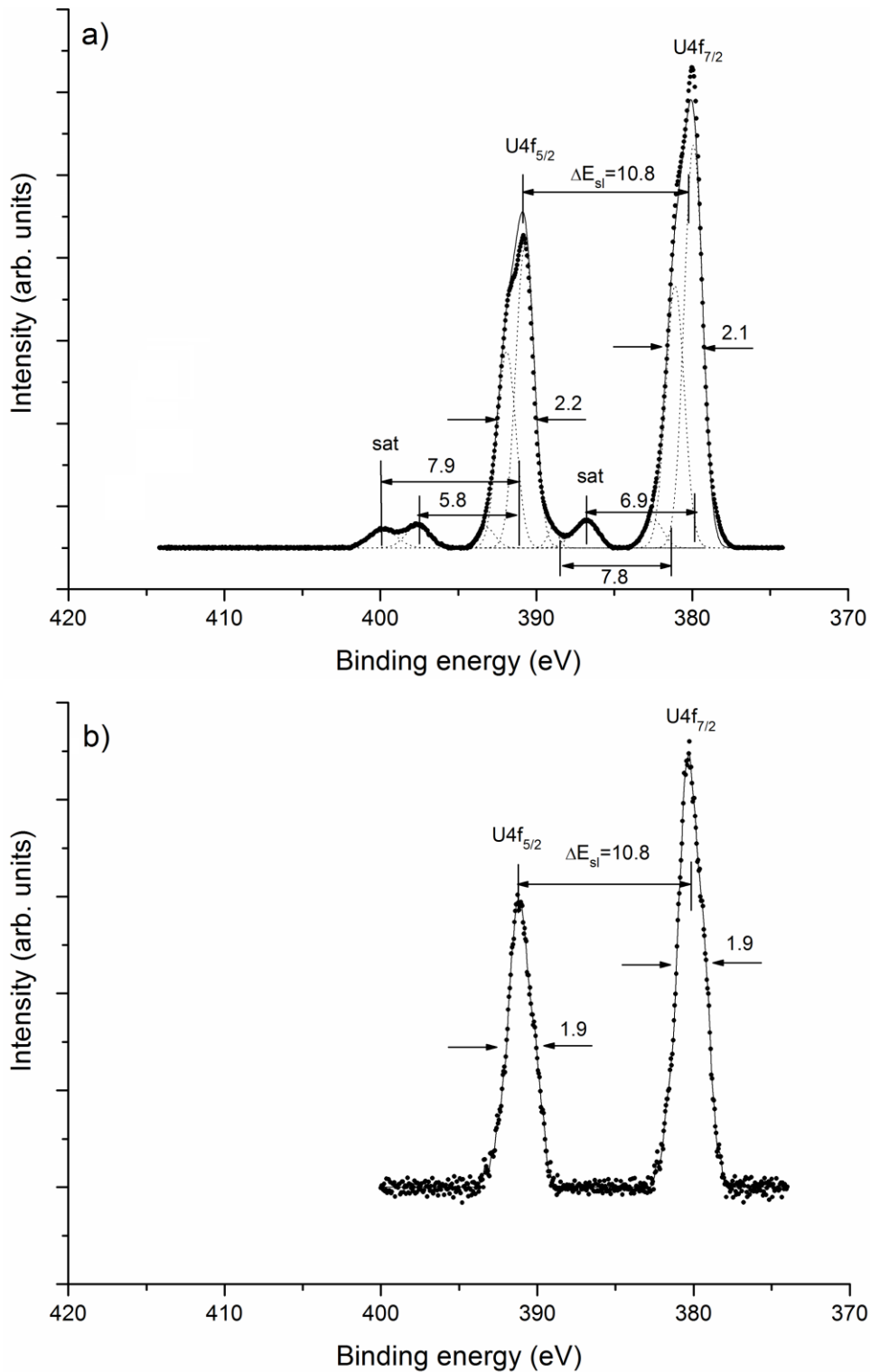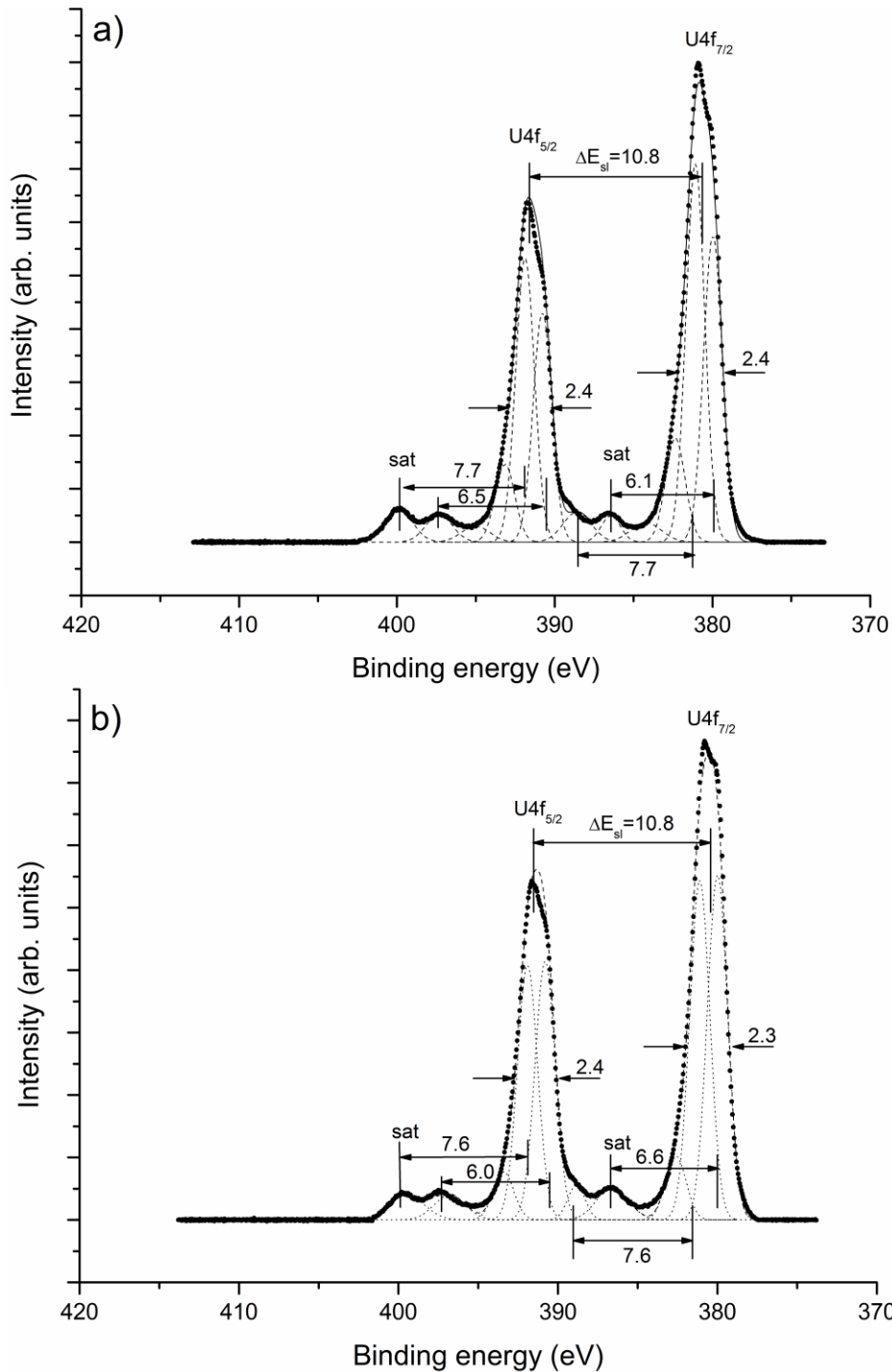
Figure 6. XPS narrow-scans of U 4f from UO_2 films: a) unirradiated surface (sample AP3); b) after $^{129}Xe^{23+}$ irradiation (92 MeV, 4.8×10^{15} ions/cm^2, sample OB3).

The environment influence causes formation of a complex oxide UO_{2+x} on the surface of the single crystal UO_2 film. As a result, oxygen is observed at the surface of the films at 530.1 eV BE participating in a metal-oxygen bond (Figure 5, Table 3). The oxygen coefficient changes from 2.8 to 3.9 in the UO_{2+x} oxide (Table 2) and exceeds possible values (from 2 to 3) for this parameter even with accounting oxygen in Nb_2O_5. Therefore, it is difficult to determine the oxygen coefficient in a UO_{2+x} oxide based on the core peak intensity of oxygen and uranium. This agrees with the previous work results.[49] However, the k_O values found based on the U 5f intensity are in a satisfactory agreement with the results obtained based on decomposition of the

U 4f spectrum for the cases, e.g., AP2, when resolution of the U 4f spectrum is relatively good (see values in the parentheses in Table 2). These values confirm experimentally that determination of the oxygen coefficient k_O based on relative U 5f intensity for UO_{2+x} has sufficient physical justification.

This complex oxide contains three different uranium ions. Results for films AP1-4 formed on the LSAT differ from those for AP5-7 formed on the YSZ. Content of uranium ions of different oxidation states in samples AP2,3 is comparable within the measurement error (see Table 2). Samples AP2 and AP3 should have the same structure and to a higher extent are single crystalline based on the XRD data. The higher content of U^{4+} ions and the lower content of U^{5+} and U^{6+} in AP2 compared to AP3 can be explained by a higher (approx. by a factor of 5) carbon content on the surface of film AP2 as compared to AP3. Possibly, this carbon coating inhibits further oxidation of the film. Samples AP1 and AP4 contain 2.8 and 3.9 oxygens per one uranium atom with $E_b(O\ 1s)\sim529.8$ eV bonded with metal (Table 3). Despite this, the k_O values for AP1 and AP4 are similar. By going from AP2,3 (UO_2 (001)) to AP4 (UO_2 preferential (111)) the value of k_O increases.

Figure 7. XPS narrow-scans of U 4f from UO_2 films: a) unirradiated surface (sample AP7); b) after $^{238}U^{31+}$ irradiation (110 MeV, 5×10^{12} ions/cm^2, sample OB7).

By going from samples AP1-4 to AP5-7 an increase in k_O values, concentration of U^{5+} and U^{6+} ions and a decrease in U^{4+} ions content is observed. Despite the difference in crystallographic orientation of the films in samples AP5-7 the amount of oxygen remains constant on them within the experimental error (Table 2). Herewith, the value of k_O increases in line AP5 (UO_2 (001)), AP7 (UO_2 (111)) and AP6 (UO_2 (110)) for which concentration of U^{4+} decreases and concentration of U^{5+} and U^{6+} ions increases.

$^{129}Xe^{23+}$ irradiation (92 MeV energy, 4.8×10^{15} ions/cm^2 fluence, penetration depth ~ 6.5 μm) of UO_2 films (OB1-4) on the LSAT substrates was conducted in order to simulate the damage from nuclear fission fragments in nuclear fuel. Mass and energy of ions used for the irradiation are typical for fission fragments. The U 5f intensities, oxygen coefficients (k_O) and ionic compositions (k, %) are given in Table 2 for each sample. In all cases the $^{129}Xe^{23+}$

irradiation causes a severe damage. This conclusion can be drawn from the facts that the structure disappears in the U 4f spectrum and the O 1s XPS peak grows significantly due to substrate oxygen in island formations with low uranium content on the substrate. This results in strong changes in UO_{2+x} composition (Table 2).

For example, the surface of unirradiated sample AP3 has the following elemental composition relative to uranium atom: $U_{1.00}O_{3.6}C_{1.8}$. The surface of complementary Xe irradiated sample OB3 has the following composition: $U_{1.00}O_{15}Ta_{3.9}C_{167}$. Calculations of the elemental compositions involved only the O 1s intensity at 530.1 eV, the Ta 4f intensity and the total C 1s intensity. The change in the surface composition can be explained by the fact that the single-crystalline film was severely damaged by Xe ions, and atoms of, for example, tantalum and oxygen from the substrate emerged to the surface. As a result, uranium oxide on the surface became amorphous. This led to decrease of intensity and destruction of the U 4f spectrum, which is employed for the quantitative ionic analysis on the basis of the U 4f BE. Since in the U 4f and U 5f BE ranges XPS peaks of other elements involved are absent, although the U 4f peak is low-intense and not structured, the technique suggested in this work (see Section C) allows an evaluation of uranium ionic composition in the studied sample (Table 2), which make this technique original.

The U 4f fine structure reflecting the OVMO structure vanishes since the chemical bond changes significantly (Figure 6b). In this case determination of the oxygen coefficient and ionic composition on the basis of the U 4f and O 1s intensities (traditional for XPS) is practically impossible. However, the technique based on the U 5f intensity, as it is shown in this work, allows one to evaluate the oxygen coefficient and ionic composition (Table 2). This is possible because the U 5f and U 4f photoionization cross-sections are high, which means that the U 5f and U 4f peaks are intense, and the U 5f and U 4f BE ranges do not contain peaks of other elements.[81]

The $^{129}Xe^{23+}$ irradiation results in a significant decrease of U^{4+} content and increase of U^{5+} and U^{6+} content (Table 2). It is especially noticeable for OB1 where U^{4+} ions are practically absent. Since the solubility of uranium ions strongly depends on the oxidation state (U^{6+} more soluble than U^{4+} by several orders of magnitude), the absence of U^{4+} in sample OB1 is supported by a higher content (~by a factor of 100) of dissolved uranium ions in deionised water as compared to samples OB2-4.

For surfaces of the unirradiated films on the YSZ substrates (AP5-7) a significant decrease of U^{4+} content and increase of U^{5+} and U^{6+} content compared to AP1-4 on the LSAT substrates was observed (Table 2). One of the reasons for this is the change in composition and structure of the lattice in the YSZ substrates compared to those in the LSAT substrates that can influence formation of a different number of defects during the growth of UO_2 single crystals. The YSZ substrates differ from the LSAT substrates by the fact that they put the UO_2 films at compression (-6.4%) due to lattice mismatch between the films and the substrates. This might lead to creation of defects in the UO_2 films. The LSAT substrate in (001) orientation gives a minor mismatch of 0.03% by putting the film at tension.

$^{238}U^{31+}$ (110 MeV, fluence 5×10^{10}, 5×10^{11} and 5×10^{12} ions/cm^2, penetration depth ~6.7 μm) irradiation of OB5-7 films on the YSZ substrates was also performed in order to study the effect of accumulating radiation damage. The surface elemental composition of UO_{2+x}, U 5f intensities, oxygen coefficients (k_O) and ionic compositions (k, %) are given in Table 2 for each sample. $^{238}U^{31+}$ irradiations do not cause a severe damage of the films (Figure 7b). This is mainly due to low fluencies. The surface elemental composition of the UO_{2+x} films, including carbon content, does not change within the experimental error.

However, the $^{238}U^{31+}$ irradiations cause changes in the ionic composition of the samples (Table 2). The oxygen coefficient (k_O) decreases compared to that for the unirradiated counter-parts. U^{4+} concentration grows, while U^{6+} concentration decreases. The error in determination of the composition of uranium ions based on decomposition of uranium peaks into components increases due to blurring of the structure in the U 4f spectra. After the irradiation the composition

of uranium ions on the surface of samples OB5-7 equalizes, what is observed during formation of stable (metastable) forms of UO_{2+x}, which is also observed after the Ar^+ etching of samples AP7 (Ar^+) (Table 2).

These data show that within the measurement error uranium quantitative ionic composition weakly, but depends on the crystallographic orientation.

Core Electron XPS Range. Hydrocarbons and water molecules that contain oxygen adsorb on the surface of the samples during the handling. The surfaces of the studied samples, as was already noted, were not cleaned with Ar^+ ions in order not to destroy its initial structure.

The O 1s spectrum of the studied samples consists of a relatively sharp peak at E_b(O 1s)=530.1 eV, Γ(O 1s) = 1.0 eV (AP3) that is typical for crystalline UO_2 (Figure 5, Table 3). At the higher BE side from the basic peak two low-intensity peaks at 531.1 eV and 531.9 eV of the surface oxygen were observed. The first peak can be attributed to the OH^- group, the other one – to the CO_3^{2-} group. After the $^{129}Xe^{23+}$ irradiation the O 1s intensity grows significantly due to the substrate oxygen (see Table 2). This causes a significant change in UO_{2+x} surface composition. The $^{238}U^{31+}$ irradiations affect the XPS structure to a smaller extent.

Results of the quantitative analysis on the basis of the U 4f and O 1s intensities show that the number of oxygen atoms in UO_{2+x} is greater than 2.8. For example, for sample AP3 it is 3.6, and for OB3 – it is 15. The corresponding k_O values calculated on the basis of the U 5f intensity 2.08 and 2.14 (Table 2). After the $^{129}Xe^{23+}$ irradiation of samples OB1-4 the oxygen coefficient k_O grows, U^{4+} content drops, U^{5+} and U^{6+} content grows. After the $^{238}U^{31+}$ irradiation of samples OB5-7 the oxygen coefficient k_O decreases, U^{4+} content grows, U^{5+} and U^{6+} content decreases. The penetration depth of xenon and uranium ions is ~6.5 µm. Since the film thickness ~150 nm, the ions penetrate through the film and stop in the substrate, thus, makes impossible to observe the xenon lines in the spectra. The xenon ions destroy the lattice, but since the fluence of uranium ions is low, uranium ions only rearrange the oxygen lattice that result in a more stable structure.

Despite the presence of hydrocarbons and oxygen-containing compounds, uranium dioxide core-electron XPS peaks are observed relatively intense and well resolved.

Thus, the U 4f XPS spectrum was observed as an intense spin-orbit split (ΔE_{sl}=10.8 eV) doublet (Figure 6a,7a, Table 3). This spectrum is structured and widened due to the presence of uranium ions of different oxidation states and contains up to 30% of intensity from the shake-up satellites. The presence of the shake-up satellites indicates the long-range ordering in the films. Destruction of the long-range order leads to vanishing of the structure and satellites (Figure 6b). Since the U 4f spectrum can contain the shake-up satellites at: ~7 (U^{4+}); ~8 (U^{5+}); ~4 and ~10 eV (U^{6+}),[50,60] this spectrum is complicated and structured (Figure 6a,7a). Having suggested that the samples contain three types of uranium ions (U^{4+}, U^{5+}, U^{6+}) and calculated their quantitative compositions on the basis of the U 5f relative intensity, the U 4f spectra were decomposed into components. The criteria of accuracy of this decomposition were the difference of the total area of the calculated and the experimental peaks and the best match with the data obtained on the basis of the U 5f intensity (Figure 6,7, Table 2). Poor resolution of the XPS spectra can lead to a high error. Results of this decomposition are given in the parenthesis in Table 2. In some cases they differ significantly from the data obtained on the basis of the U 5f intensity. Parameters of the peaks and satellites for uranium ions are given in Table 3. The peaks of uranium ions of different oxidation states were suggested to have the same FWHMs. The smallest FWHM was Γ(U $4f_{7/2}$)=1.4 eV. The narrowest U 4f peak was expected from the $U(5f^0)^{6+}$ ions that do not have the U 5f electrons responsible for the possible widening due to the multiplet splitting.

Indeed, for reference samples of $PbUO_4$ and $BaUO_4$ the U $4f_{7/2}$ peaks are 1.1 and 1.2 eV wide, respectively. So, having neglected the U $4f_{7/2}$ multiplet splitting, one can expect the U $4f_{7/2}$ peak of the monophase UO_2 (CaF_2) single crystal to be 1.1 eV wide. Therefore, the total FWHM of the U $4f_{7/2}$ peak Γ(U $4f_{7/2}$) measured relative to Γ(C 1s = 1.3 eV) is an important qualitative characteristic (Table 3). Depending on the concentrations of included uranium ions in the studied films, the shape of the U 4f peak will change. Qualitative correlation of the total U $4f_{7/2}$ FWHM

with concentrations of uranium ions of different oxidation states has to be observed. Thus, for OB1,4 films U^{4+} concentrations are significantly lower, and the $\Gamma(U\ 4f_{7/2})$ are also lower comparing to those of AP1,4 films (Table 2,3).

The C 1s spectrum of the studied samples consists of the basic peak at $E_b=285.0$ eV attributed to saturated hydrocarbons, the peak at 286.5 eV attributed to carbon connected with oxygen and the peak at 288.7 eV associated with the CO_3^{2-} group on the surface (Figure 8). After the $^{129}Xe^{23+}$ irradiation the C 1s intensities grow. $^{238}U^{31+}$ irradiation practically does not cause any changes in the C 1s intensity.
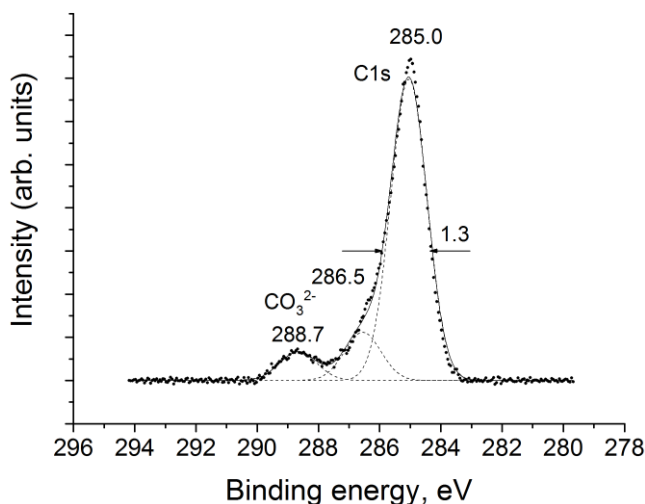
Figure 8. An XPS narrow-scan of C 1s from a UO_2 film (samples AP3).

The error in the quantitative elemental and ionic analysis of the studied samples grows because the XPS spectra of the core levels exhibit extra structure due to the multiplet splitting and secondary electronic processes (many-body perturbation and dynamic effect). Since the many-body perturbation results in shake-up satellites at the higher BE side from the main peaks, satellite intensities can be partially taken into account. The dynamic effect can be hardly taken into account, but its probability is pretty low in the considered spectra. All of the above can increase the error in the elemental and ionic analysis by about ±5%.

This work evaluated the oxygen coefficient for oxides UO_{2+x} on the basis of the U $4f_{7/2}$ and O 1s intensities (Table 2 and Figures 5 and 6). As was mentioned above, oxygen adsorption at the surface makes practically impossible a correct evaluation of the oxygen coefficient for UO_{2+x} (see Table 2). Since the ratio n_O/n_U of oxygen, n_O, and uranium, n_U, number of atoms changes in the range 2.8 to 3.9, thus, clusters with an excess of oxygen can form on the surface. Treatment with Ar^+ ions of the surface of sample AP7 for 120 sec leads to removal of the excessive oxygen and the value ($UO_{1.98}$), found based on the U $4f_{7/2}$ and O 1s intensities, is close to 2.0 ± 0.1. However, the value of k_O found based on the U 5f relative intensity electrons reduced only to 2.11 and not to 2.00 as should be expected. This is related, possibly, to the fact that annealing of the sample did not take place to restore its UO_2 (CaF_2) lattice presence in a vacuum of the chamber.

The $^{129}Xe^{23+}$ irradiation of the uranium oxide films damaged the surface significantly. The U 4f spectrum smears and the shake-up satellites vanish. This confirms the disappearance of the regular crystal structure in the samples (Figure 6b). In this case, the ionic analysis of the film's surface is practically impossible on the basis of the U 4f and O 1s parameters. A significant decrease of the U 5f intensity takes place due to the change in the surface ionic composition. Despite a severe damage of the surface, it is possible to evaluate the ionic composition on the basis of the U 5f intensity. Thus, the U^{4+} content drops while the U^{5+} and U^{6+} content grows significantly (see Table 2). On the basis of these data one can conclude that $^{129}Xe^{23+}$ irradiation leads to both the long-range order destruction and to the short-range order destruction of the uranium close environment, which results in increase of uranium oxidation

state and restructuring of oxygen ions in the uranium environment. The $^{238}U^{31+}$ irradiations lead to a partial long-range order destruction and formation of lattice defects. X-ray diffraction study showed that the ion irradiations resulted in diffraction peak broadening due to a decrease in the size of coherent scattering domains that is consistent with destruction of the long-range order.

OKLL Auger Spectral Structure of Uranium Dioxide Film (AP3). The valence band XPS of uranium dioxide film (AP3) and the calculation results were used for a qualitative explanation of the Auger O KLL spectra structure from this film (Figures 3 and 8).

The O KLL Auger spectrum of Al_2O_3, where the O 2s shell participates weakly in the IVMO formation, consists of three well resolved low structured ~9 eV wide components reflecting the $OKL_{2-3}L_{2-3}$ (O 1s ← O 2p), OKL_1L_{2-3} (O 1s ← O 2s,2p) and OKL_1L_1 (O 1s ← O 2s) electronic transitions.[82] Relative intensities of these peaks given as the ratios of Auger peaks intensities to the O 1s XPS peak intensity are important fundamental values. They allow a quantitative comparison of partial electronic densities, for e.g., of the O 2p states on oxygen ions in different oxides.[82]

The O KLL Auger spectrum of uranium dioxide film (sample AP3) measured in this work consists of three structured bands (Figure 9). This structure is partially due to the oxygen-containing impurities on the sample surface. Despite this fact, a qualitative interpretation of this spectrum is possible. In the O KLL Auger spectrum of AP3 the $OKL_{2-3}L_{2-3}$ (O 1s ← O 2p) peak at 973.8 eV and Γ~3.7 eV reflects the density of the filled O 2p states (Figure 9). The FWHM of this peak qualitatively agrees with the sum of the XPS O 1s FWHM (Γ=1.0 eV, Figure 5) and the O 2p band FWHM (Γ~4.4 eV, Figure 3). The OKL_1L_{2-3} (O 1s ← O 2s,2p) band reflecting the O 2p and O 2s densities of states (DOS) is structured. The OKL_1L_1 (O 1s ← O 2s) band reflecting the O 2s DOS is also structured due to participation of the O 2s electrons in the IVMO formation. This band is ~15 eV wide, which is comparable with the IVMO XPS band FWHM. This confirms the participation of the O 2s AOs in the IVMO formation (Figures 3 and 8). These results agree with the Auger O KLL results for UO_2 (ref 83).
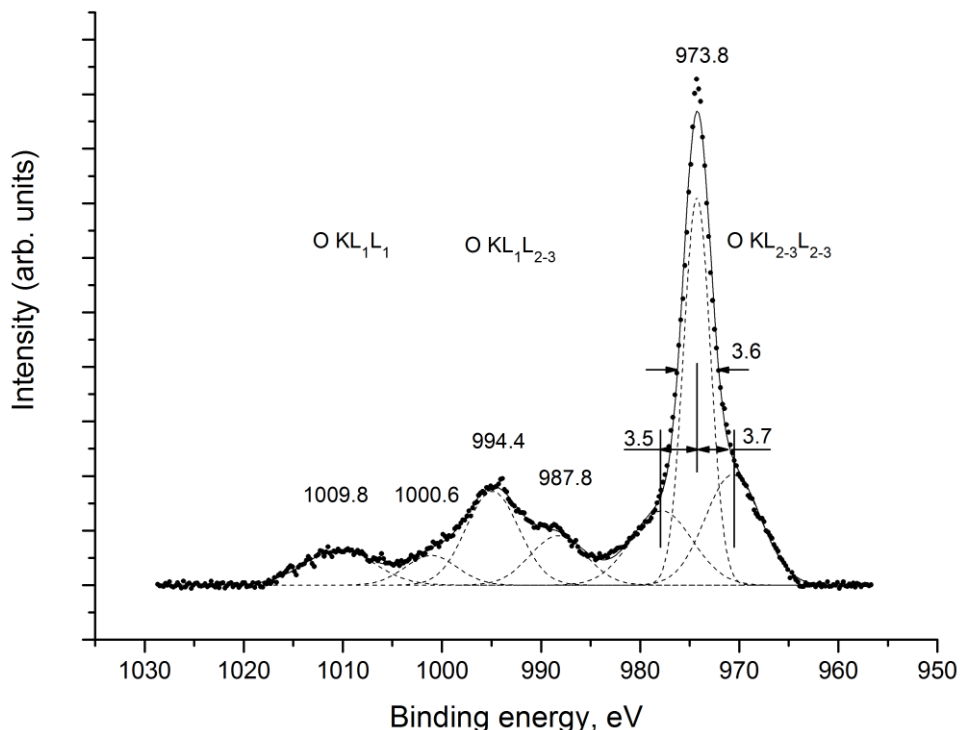
Figure 9. An Auger spectrum of O KLL from a UO_2 film (sample AP3).

CONCLUSIONS

XPS determination of the oxygen coefficient $k_O=2+x$ and ionic (U^{4+}, U^{5+} and U^{6+}) composition of oxides UO_{2+x} formed on the surfaces of differently oriented (hkl) planes of thin UO_2 films on the LSAT and YSZ substrates was performed. The U 4f and O 1s core-electron peak intensities as well as the U 5f relative intensity before and after the $^{129}Xe^{23+}$ (92 MeV, fluence 4.8×10^{15} ions/cm^2) and $^{238}U^{31+}$ (110 MeV, fluence 5×10^{10}, 5×10^{11} and 5×10^{12} ions/cm^2) irradiations were employed.

It was found that the presence of uranium dioxide film in air results in formation of oxide UO_{2+x} on the surface with mean oxygen coefficients k_O from 2.07 to 2.11 on the LSAT and from 2.17 to 2.23 on the YSZ substrates. These oxygen coefficients depend on the nature of the substrate and weakly on the crystallographic orientation.

On the basis of the spectral parameters it was established that uranium dioxide films AP2,3 on the LSAT substrates have closest to stoichiometric values of the k_O, and from the XRD and EBDS results it follows that these films have a regular single crystal structure. The XRD and EBSD results indicate that uranium oxide films one the YSZ substrates have single crystal structure, however, they have the highest oxygen coefficient k_O. This difference, possibly, related to the different nature of the substrates.

The $^{129}Xe^{23+}$ irradiation (92 MeV, fluence 4.8×10^{15} ions/cm^2) of uranium dioxide films on the LSAT substrates was shown to destroy both long range ordering and uranium close environment, which results in increase of uranium oxidation state and regrouping of oxygen ions in the uranium close environment. The $^{238}U^{31+}$ irradiations (110 MeV, fluence 5×10^{10}, 5×10^{11} and 5×10^{12} ions/cm^2) of uranium dioxide films on the YSZ substrates was shown to form the lattice damage only with partial destruction of the long range ordering. This is mainly due to low fluencies. However, the $^{238}U^{31+}$ irradiations caused changes in the ionic composition of the samples: an increase in U^{4+} concentration and a decrease in U^{6+} concentration were observed, hence the oxygen coefficient (k_O) decreased compared to that for the unirradiated counter-parts.

AUTHOR INFORMATION

Corresponding Author
*Present address: Department of Earth Sciences, University of Cambridge, Downing Street, Cambridge, CB2 3EQ, United Kingdom, Tel: +44 1223 768357, E-mail: apopel@cantab.net.

REFERENCES

(1) He, H.; Qin, Z.; Shoesmith D. W. *Electrochim. Acta* **2010**, *56*, 53–60.

(2) Matzke, Hj. *J. Nucl. Mater.* **1992**, *190*, 101–106.

(3) Sonoda, T.; Kinoshita, M.; Ishikawa, N.; Sataka, M.; Iwase, A.; Yasunaga, K. *Nucl. Instr. and Meth. in Phys. Res. B* **2010**, *268*, 3277–3281.

(4) Matzke, Hj.; Lucuta, P. G.; Wiss, T. *Nucl. Instr. and Meth. in Phys. Res. B* **2000**, *166–167*, 920–926.

(5) Wiss, T.; Matzke, Hj.; Trautmann, C.; Toulemonde, M.; Klaumünzer, S. *Nucl. Instr. and Meth. in Phys. Res. B* **1997**, *122*, 583–588.

(6) Opel, K.; Weiß, S.; Hübener, S.; Zänker, H.; Bernhard, G. *Radiochim. Acta* **2007**, *95*, 143–149.

(7) He, H.; Zhu, R. K.; Qin, Z.; Keech, P.; Ding, Z.; Shoesmith, D. W. *J. Electrochem. Soc.* **2009**, *156*, C87–C94.

(8) Shoesmith D. W.; Sunder, S. *J. Nucl. Mater.* **1992**, *190*, 20–35.

(9) Andersson, D. A.; Uberuaga, B. P.; Nerikar, P. V.; Unal, C.; Stanek, C. R. *Phys. Rev. B* **2011**, *84*, 054105.

(10) Andersson, D. A.; Lezama, J.; Uberuaga, B. P.; Deo, C.; Conradson, S. D. *Phys. Rev. B* **2009**, *79*, 024110.

(11) Crocombette, J.-P.; Torumba, D.; Chartier, A. *Phys. Rev. B* **2011**, *83*, 184107.

(12) Wang, J.; Ewing, R. C.; Becker, U. *Phys. Rev. B* **2013**, *88*, 024109.

(13) Geng, H. Y.; Chen, Y.; Kaneta, Y.; Kinoshita, M. *Phys. Rev. B* **2007**, *75*, 054111.

(14) Rak, Zs.; Ewing, R. C.; Becker, U. *Surf. Sci.* **2013**, *608*, 180–187.

(15) Wang, D.; van Gunstren, W. F.; Chain, Z. *Chem. Soc. Rev.* **2012**, *41*, 5836–5865.

(16) Boettger, J. C.; Ray, A. K. *Int. J. Quantum Chem.* **2002**, *90*, 1470–1477.

(17) Fuggle, J. C.; Mårtensson, N. *J. Electron Spectrosc. Relat. Phenom.* **1980**, *21*, 275–281.

(18) Moser, H. R.; Delley, B.; Schneider, W. D.; Baer, Y. *Phys. Rev. B* **1984**, *29*, 2947.

(19) Fu, X.; Wang, X.; Zhao, Z.; Yu, Y. *Surf. Rev. Lett.* **2003**, *10*, 381–386.

(20) Moor, K. T.; van der Laan, G. *Rev. Mod. Phys.* **2009**, *81*, 235.

(21) Opeil, C. P.; Schulze, R. K.; Manley, M. E.; Lashley, J. C.; Hults, W. L.; Hanrahan, Jr., R. J.; Smith, J. L.; Mihaila, B.; Blagoev, K. B.; Albers, R. C.; Littlewood, P. B. *Phys. Rev. B* **2006**, *73*, 165109.

(22) Kudin, K. N.; Scuseria, G. E.; Martin, R. L. *Phys. Rev. Lett.* **2002**, *89*, 266402.

(23) Prodan, I. D.; Scuseria, G. E.; Martin, R. L. *Phys. Rev. B* **2007**, *76*, 033101.

(24) Prodan, I. D.; Scuseria, G. E.; Martin, R. L. *Phys. Rev. B* **2006**, *73*, 045104.

(25) Dorado, B.; Amadon, B.; Freyss, M.; Bertolus, M. *Phys. Rev. B* **2009**, *79*, 235125.

(26) Gubanov, V. A.; Rosen, A.; Ellis, D. E. *J. Phys. Chem. Solids.* **1979**, *40*, 17–28.

(27) Suzuki, C.; Nishi, T.; Nakada, M.; Akabori, M.; Hirata, M.; Kaji, Y. *J. Quantum Chem.* **2009**, *109*, 2744–2752.

(28) Wen, X.-D.; Martin, R. L.; Roy, L. E.; Scuseria, G. E.; Pudin, S. P.; Batista, E. R.; McGleskey, T. M.; Scott, B. L.; Bauer, E.; Joyce, J. J.; Durakiewicz, T. *J. Chem. Phys.* **2012**, *137*, 154707.

(29) Wen, X.-D.; Martin, R. L.; Henderson, T. M.; Scuseria, G. E. *Chem. Rev.* **2013**, *113*, 1063–1096.

(30) Suzuki, C.; Nishi, T.; Nakada, M.; Tsuru, T.; Akabori, M.; Hirata, M.; Kaji, Y. *J. Phys. Chem. Solids* **2013**, *74*, 1769–1774.

(31) Yang Y.; Zhang, P. *J. Appl. Phys.* **2013**, *113*, 013501.

(32) Yun, Y.; Rusz, J.; Suzuki, M.-T.; Oppeneer, P. M. *Phys. Rev. B* **2011**, *83*, 075109.

(33) Shi, H.; Chu, M.; Zhang, P. *J. Nucl. Mater.* **2010**, *400*, 151–156.

(34) Petit, L.; Svane, A.; Szotek, Z.; Temmerman, W. M.; Stocks, G. M. *Phys. Rev. B* **2010**, *81*, 045108.

(35) Naegele, J. R.; Ghijsen, J.; Manes, L. *Struct. Bond.* **1985**, *59/60*, 197–262.

(36) Seibert, A.; Gouder, T.; Huber, F. *Radiochim. Acta* **2009**, *97*, 247–250.

(37) Gouder, T.; Seibert, A.; Havela, L.; Rebizant, J. *Surf. Sci.* **2007**, *601*, L77–L80.

(38) Idriss, H. *Surf. Sci. Rep.* **2010**, *65*, 67–109.

(39) Miserque, F.; Gouder, T.; Wegen, D. H.; Bottomley, P. D. W. *J. Nucl. Mater.* **2001**, *298*, 280–290.

(40) Burrell, A. K.; McCleskey, T. M.; Shukla, P.; Wang, H.; Durakiewicz, T.; Moore, D. P.; Olson, C. G.; Joyce, J. J.; Jia, Q. *Adv. Mater.* **2007**, *19*, 3559–3563.

(41) Beatham, N.; Orchard, A. F.; Thornton, G. *J. Electr. Spectr. Relat. Phenom.* **1980**, *19*, 205–211.

(42) Teterin, Yu. A.; Maslakov, K. I.; Ryzhkov, M. V.; Traparid, O. A.; Vuktevie, L.; Teterin, A. Yu.; Panov, A. D. *Radiochemistry* **2005**, *47*, 215–224.

(43) Chadwick D.; Graham, J. *Nature Phys. Sci.* **1972**, *237*, 127–128.

(44) Teterin, Yu. A.; Kulakov, V. M.; Baev, A. S.; Zelenkov, A. G.; Nevzorov, N. B.; Melnikov, I. V.; Sreltsov, V. A.; Mashirov, L. G.; Suglobov, D. N. *Doklady Akademii Nauk SSSR (Reports of Academy of Science of USSR)* **1980**, *255*, 434–437 (in Russian).

(45) Teterin, Yu. A.; Kulakov, V. M.; Baev, A. S.; Nevzorov, N. B.; V.Melnikov, I.; Streltsov, V. A.; Mashirov, L. G.; Suglobov, D. N.; Zelenkov, A. G. *Phys. Chem. Minerals* **1981**, *7*, 151–158.

(46) Miyake, C.; Sakurai, H.; Imoto, S. *Chem. Phys. Lett.* **1975**, *36*, 158–160.

(47) Allen G. C.; Holmes, N. R. *Can. J. Appl. Spectrosc.* **1993**, *38*, 124–130.

(48) Van den Berghe, S.; Miserque, F.; Gouder, T.; Gaudreau, B.; Verwerft, M. *J. Nucl. Mater.* **2001**, *294*, 168–174.

(49) Teterin, A. Yu.; Teterin, Yu. A.; Maslakov, K. I.; Batuk, O. N.; Kalmykov, S. N.; Zakharova, E. V. *Radiochemistry*, **2009**, *51*, 450–457.

(50) Teterin Yu. A.; Teterin, A. Yu. *Russ. Chem. Rev.* **2004**, *73*, 541–580.

(51) Ulrich, K.-U.; Ilton, E. S.; Veeramani, H.; Sharp, J. O.; Bernier-Latmani, R.; Schofield, E. J.; Bargar, J. R.; Giammar, D. E. *Geochim. Cosmochim. Acta* **2009**, *73*, 6065–6083.

(52) Veal B. W.; Lam D. J. *Phys. Rev. B* **1974**, *10*, 4902.

(53) Veal, B. W.; Diamond, H.; Hoekstra, H. R. *Phys. Rev. B* **1977**, *15*, 2929.

(54) Veal, B. W.; Lam, D. J.; Diamond, H. *Physica B+C* **1977**, *86-88*, 1193–1194.

(55) Cox L. E.; Farr, J. D. *Phys. Rev. B* **1989**, *39*, 11142.

(56) Gouder, T.; Colmenares, C.; Naegele, J. R.; Verbist. J. *Surf. Sci.* **1989**, *235*, 280–286.

(57) Stumpf, S.; Seibert, A.; Gouder, T.; Huber, F.; Wiss, T.; Römer, J. *J. Nucl. Mater.* **2009,** *385,* 208–211.

(58) Chen, Q.; Lai, X.; Bai, B.; Chu, M. *Appl. Surf. Sci.* **2010**, *256*, 3047–3050.

(59) Teterin Yu. A.; Baev, A. S. *Rentgenovskaya Fotoelectronnaya Spectroscopiya Soedinenii Legkikh Aktinoidov (X-Ray Photoelectron Spectroscopy of Light Actinide Compounds)*; TsNIIatominform: Moscow, p. 104, 1986 (in Russian).

(60) Ilton E. S.; Bagus, P. S. *Surf. Interface Anal.* **2011**, *43*, 1549–1560.

(61) Teterin, A. Yu.; Ryzhkov, M. V.; Teterin, Yu. A.; Panov, A. D.; Nikitin, A. C.; Ivanov, K. E.; Utkin, I. O. *Radiochemistry,* **2002**, *44*, 224–233.

(62) Ilton, E. S.; Haiduc, A.; Cahill, C. L.; Felmy, A. R. *Inorg. Chem.* **2005**, *44*, 2986–2988.

(63) Ilton, E. S.; Bagus, P. S. *Phys. Rev. B* **2005**, *71*,195121.

(64) Pireaux, J. J.; Riga, J.; Thbaut, E.; Tenret-Noel, C.; Caudano, R.; Verbist, J. J. *Chem. Phys.* **1977**, *22*, 113–120.

(65) Yarzhemsky, V. G.; Nefedov, V. I.; Trzhaskovskaya, M. B.; Band, I. M.; Teterin, Yu. A.; Teterin, A. Yu. *J. Surf. Invest.: X-ray, Synchrotron Neutron Tech.* **2001**, *7*, 32 (in Russian).

(66) Yarzhemsky, V. G.; Nefedov, V. I.; Trzhaskovskaya, M. B.; Band, I. M.; Szargan, R. *J. Electron Spectrosc. Relat. Phenom.* **2002**, *123*, 1–10.

(67) Teterin, Yu. A.; Ivanov, K. E.; Teterin, A. Yu.; Lebedev, A. M.; Utkin, I. O.; Vukchevich, L. *J. Electron Spectrosc. Relat. Phenom.* **1999**, *101-103*, 401–405.

(68) Teterin, A. Yu.; Ryzhkov, M. V.; Teterin, Yu. A.; Maslakov, K. I.; Reich, T.; Molodtsov, S. L. *J. Struct. Chem.* **2011**, *52*, 295–303.

(69) Teterin Yu. A.; Teterin, A. Yu. *Nucl. Technol. Radiat.* **2004**, *19*, 3–14.

(70) Tobin J. G.; Yu, S.-W. *Phys. Rev. Lett,* **2011**, *107*, 167406.

(71) Bao, Z.; Springell, R.; Walker, H. C.; Leiste, H.; Kuebel, K.; Prang, R.; Nisbet, G.; Langridge, S.; Ward, R. C. C.; Gouder, T.; Caciuffo, R.; Lander, G. H. *Phys. Rev. B* **2013**, *88*, 134426.

(72) Chakoumakos, B. C.; Schlom, D. G.; Urbanik, M.; Luine, J. *J. Appl. Phys.* **1998**, *83*, 1979–1982.

(73) Strehle, M. M.; Heuser, B. J.; Elbakhshwan, M. S.; Han, X.; Gennardo, D. J.; Pappas, H. K.; Ju, H. *Thin Solid* Films **2012**, *520*, 5616–5626.

(74) Ziegler, J. F.; Biersack, J. P.; Ziegler, M. D. *The Stopping and Range of Ions in Matter*; SRIM Co.: Chester, Maryland, U.S.A., 2008.

(75) Shirley, D. A. *Phys. Rev. B* **1972**, *5*, 4709.

(76) Gouder T.; Havela, L. *Mikrochim. Acta* **2002***, 138*, 207–215.

(77) Frazer, B. C.; Shirane, G.; Cox, D. E.; Olsen, C. E. *Phys. Rev.* **1965**, *140*, A1448.

(78) Rafalsky, R. P.; Alexeev, V. A.; Ananyeva, L. A. *Geokhimiya (Geochemistry)* **1979**, *11*, 1601 (in Russian).

(79) Stubbs, J. E.; Chaka, A. M.; Ilton, E. S.; Biwer, C. A.; Engelhard, M. H.; Bargar, J. R.; Eng, P. J. *Phys. Rev. Lett.* **2015**, *114*, 246103.

(80) Il'in, E. G.; Parshakov, A. S.; Teterin, A. Yu.; Maslakov, K. I.; Teterin, Yu. A. *Russ. J. Inorg. Chem.* **2011**, *56*, 1788–1793.

(81) Scofield, J. H. *J. Electr. Spectrosc. Relat. Phenom* **1976**, *8*, 129–137.

(82) Teterin, Y. A.; Ivanov, K. E.; Teterin, A. Y.; Lebedev, A. M.; Utkin, I. O.; Vukchevich, L. *J. Electron Spectrosc. Relat. Phenom.* **1999**, *101–103*, 401–405.

(83) Teterin Yu. A.; Teterin, A. Yu. *Radiochemistry* **2005**, *47*, 440–446.
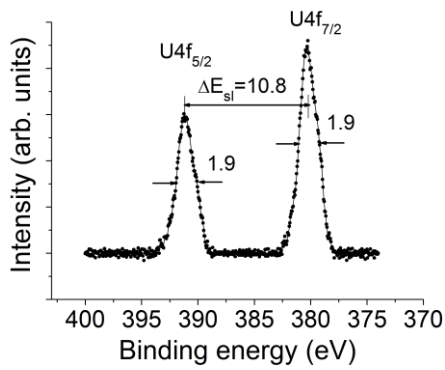
For Table of Contents Only

An effective technique for determination of ionic composition (U^{4+}, U^{5+}, U^{6+}) and oxygen coefficient in UO_{2+x} was introduced and developed. This method is based on the U 5f and U 4f XPS peak intensities. The suggested technique allowed a determination of the surface ionic uranium composition and the oxygen coefficient in heavily $^{129}Xe^{23+}$ irradiated (92 MeV, 4.8×10^{15} ions/cm^2) uranium dioxide thin films, when the traditional approach was impossible to be employed.